Applied Mechanics and Materials Vols. 152-154 (2012) pp 1806-1813
Online available since 2012/Jan/24 at www.scientific.net

doi:10.4028/www.scientific.net/AMM.152-154.1806

Large Eddy Simulation of Wind Loads on a Low-Rise Structure and Comparison with Wind Tunnel Results

Isam Janajreh[1,a], and Emil Simiu[2,b]

[1]Masdar Institute of Science and Technology, Abu Dhabi, United Arab Emirates

[2]National Institute of Standard and Technology, Gaithersburg, USA

[a]ijanajreh@masdar.ac.ae, [b]emil.simiu@nist.gov

Keywords: Aerodynamics, Computational Fluid Dynamics (CFD), Large Eddy Simulation, Wind Engineering

Abstract. This work presents estimates of time histories of pressure coefficients at several taps on the roof of a 1/200 model of a 200 x 100 x 20 ft low-rise building with a 1/24 slope gable roof building. The estimates were obtained by large eddy simulation (LES). The first and second moments as well as peaks for the time histories are compared with those obtained in boundary layer wind-tunnel measurements at the University of Western Ontario. It is noted that the computation times required to obtain records of length comparable to wind tunnel records are at present prohibitively large.

Introduction. Computational Fluid Dynamics (CFD), referred as virtual wind tunnel" is becoming a viable tool for obtaining aerodynamic data that can be used confidently for structural design. In recent years higher resolution schemes and faster solver algorithms have been developed, including, multi-grid solution accelerators, higher order discretization algorithms, and arbitrary Lagrangian-Eulerian formulation. Computational hardware advances, i.e., augmentation in processor speed, improvements in parallel computation and digital storage capabilities, are important steps toward making CFD an increasingly useful tool. However, wind engineering applications continue to pose a challenge to CFD owing to the difficulty of modeling turbulence in the atmospheric boundary layer and in regions around bluff bodies where wake flows, flow separation and reattachment, vortex shedding, and free shear layers occur. Transient flows render data processing and management an even more difficult task. Reynolds Average Navier-Stokes (RANS) turbulence models have demonstrated their efficiency and accuracy when applied to isotropic turbulent flow fields. Their usefulness, however, is not established for applications to flows around bluff bodies embedded within the atmospheric boundary layer. RANS turbulence treats both large- and small-scale turbulence similarly. Theory and experiments, in contrast, suggest that only the small turbulent scales are universal. Direct Numerical Simulation (DNS) and Large Eddy Simulations (LES) are alternatives, albeit costly, to RANS that can model satisfactorily the low frequency scales. Temporal and spatial resolutions, down to the viscous dissipation scale, i.e., the Kolmogorov scale ($\eta = L.\,\mathrm{Re}^{\frac{-3}{4}}$, L is the characteristic length of a given Reynolds number (Re)), would place high demands on DNS since to solve the flow field down to this high resolution scale the required number of nodes for one dimension would be $Re^{3/4}$; and $Re^{\,9/4}$ for three dimensions. For the problem at hand where Re = 38,100, the corresponding number of nodes is 1.23×10^{10}, which is intractable given the current computational capabilities. Therefore, DNS is useful primarily for understanding the turbulence physics at low Reynolds numbers and gaining insight into the development and assessment of turbulence closure models. The calculations must accommodate both the large scales that are imposed by external effects and the small scale associated with viscous dissipation. LES uses the equations of motion of the flow to model its large scale motions. However, unlike DNS, scales comparable to or smaller than the grid size are modeled by implementing a universal turbulence model. In wind tunnels, large upstream spires and roughness fetches create turbulent flows that simulate the atmospheric boundary layer flow with various degrees of success. As comparisons between results obtained by various wind tunnel laboratories show, such simulations are difficult to achieve, particularly at low elevations of interest for low-rise building design [1]. The sampling frequency f for the model and the prototype are related such as $(H\,f\,/\,V)_m = (H\,f\,/\,V)_p \quad or \quad f_m \;= \lambda\, f_p V_m\,/\,V_p)$ where H denotes the characteristic length (e.g., the building height), f denotes the sampling frequency, and V denotes the mean wind velocity at the reference height; λ represents the scale ratio, and the subscripts m and p represent model and prototype scales, respectively. Records on the order of one minute are typical for wind tunnel tests. Owing to current computational limitations, in this work shorter records will be sought. Such shorter records can be useful for research purposes, even though the sampling errors inherent in them can be relatively large [2].Solving for one second long of 1/200 model comprising a 1,200,000 cell requires 6 weeks period utilizing a quad 2.4GHz processor. The sampling time and solution stability are constrained by the dilation wave speed, via the Courant-Friedrichs-Lewy (CFL) condition [3], that is, $CFL \equiv \Delta t\,.V_H\,/\,\min(dx, dy, dz) \le 1$, where Δt is the time step, V_H is the local flow speed, and dx, dy and dz are the cell dimensions. The desired residual values for continuity and momentum are 10^{-6} and 10^{-8}, respectively. This work consists of computing pressure time histories at points located on the building roof, and carrying out comparisons with corresponding pressure tap data obtained at the Boundary Layer Wind Tunnel Laboratory of the University of Western Ontario [4]. Fig. 1, show the main characteristics of the flow field around a low-rise structure immersed in the ABL, i.e. presence of stagnation, standing vortices, separation, von Karman's vortex street, and a pronounced wake. The flow is turbulent, non-homogeneous and anisotropic. As the common eddy viscosity models of the κ−ε and κ−ω type overestimate turbulence production near the separation regions [5], the feasibility of LES to study bluff body aerodynamics induced by ABL flow over low-rise structures is pursued.

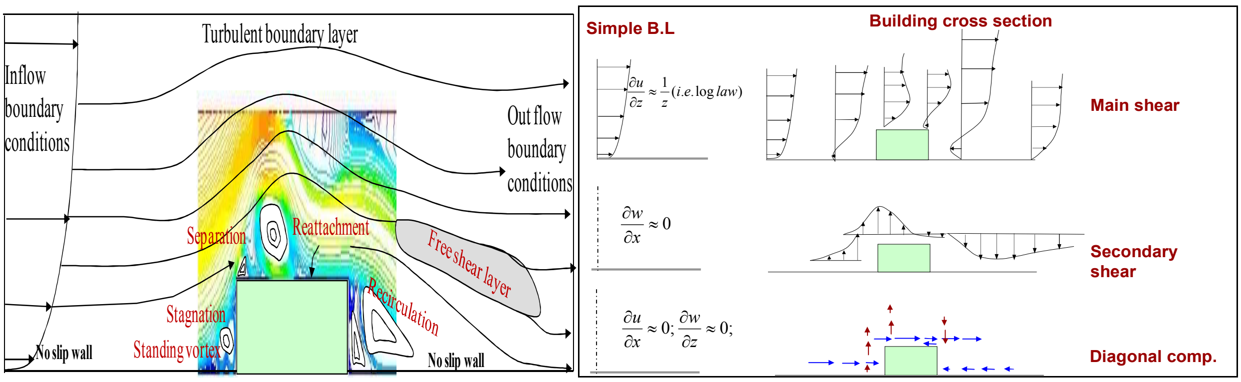

Fig. 1. Characteristic of the flow around low rise structure.

Governing System and Turbulent Modeling via Large Eddy Simulation. The Navier-Stokes equations which govern the flow are statements of conservation of mass (continuity), and momentum. Unlike the RANS turbulence modeling, LES implements a simpler model and is inherently transient. It allows explicit resolution of the large-scale turbulent motion while separately modeling small-scale turbulence. The dependent flow field variables are all written in the form: $\phi_i(\vec{x},t) = \overline{\phi}_i(\vec{x},t) + \phi'_i(\vec{x},t)$ where the bar indicates the resolved scale and the prime indicates the subgrid scale. The large scale field is the result of filtering the flow field with a filter kernel G(x,ζ;Δ), e.g., a Box, Gaussian, or cut-off filter [6]. The resulting flow field is expressed as:

$$Filter: \quad \overline{u}_i(\vec{x},t) = \int G(\vec{x},\vec{\varsigma};\Delta)\, u_i(\vec{\varsigma},t)\, d^3\vec{\varsigma} \tag{1}$$

$$Continuity: \quad \frac{\partial \overline{\rho}}{\partial t} + \frac{\partial \overline{u}_i}{\partial \overline{x}_i} = 0 \tag{2}$$

Momentum : $\frac{\partial \overline{u}_i}{\partial t}+\frac{\partial}{\partial x_j}(\overline{u}_i\overline{u}_j)=-\frac{1}{\rho}\frac{\partial \overline{p}}{\partial x_i}+\frac{\partial}{\partial x_j}\left(\nu\frac{\partial \overline{u}_i}{\partial x_j}\right)-\frac{\partial \tau_{ij}}{\partial x_j}$ (3)

where G is the spatial normalized ($\int G(\vec{x},\vec{\varsigma};\Delta)\, d^3\vec{\varsigma}=1$) filter operator at $\vec{x}$ over the defined cell space of $\vec{\varsigma}$, Δ represents the bandwidth filter parameter that characterizes individual cell mesh width, and ν is the kinematics viscosity. The subgrid scale turbulent stress tensor τ_{ij} is expressed as:

$\tau_{ij}=\overline{u}_i\overline{u}_j-\overline{u_i u_j}$ (4)

The filtered Navier-Stokes equation will contain large scale terms with the overbar symbol and small scale terms with the prime symbol. The prime terms are referred to as subgrid scale terms (SGS), and will take the form of Reynolds stresses. To assure closure of the governing system of equations, the effect of the small scale velocity components needs to be modeled. At this point, SGS (τ_{ij}) is unknown and requires a turbulent closure model. The three-dimensional Smagorinsky Eddy Viscosity model is used. It implements the following linear relation between the filtered SGS tensor (τ_{ij}) and the filtered strain rate tensor (s_{ij}) such that $\tau_{ij}=2\nu_t s_{ij}-\frac{2}{3}\tau_{kk}\delta_{ij}$ where ν_t is the turbulent kinematic viscosity, and the strain rate tensor s_{ij} is the resolved field defined as $s_{ij}=\frac{1}{2}(\frac{\partial \overline{u}_i}{\partial x_j}+\frac{\partial \overline{u}_j}{\partial x_i})$

Above τ_{kk} is the isotropic part of the subgrid-scale stresses and is added to the filtered pressure term. The turbulent kinematic viscosity ν_t, has the dimensions LV, where L and V are a length scale and a velocity scale, respectively [7] proposed the expression $\nu_t=c_s\Delta^2\sqrt{s_{ij}s_{ij}}$, where Δ is the filter band width, s_{ij} is the strain tensor (whose dimension is $[T]^{-1}$), and c_s is a non-dimensional factor determined experimentally. Accordingly, the turbulent kinetic energy κ and turbulent dissipation rate ε are expressed as $k=c_k\Delta^2(s_{ij}s_{ij})$ and, $\varepsilon=c_\varepsilon k^{3/2}/\Delta=c_\varepsilon c_k^{3/2}\Delta(s_{ij}s_{ij})^{3/2}$, respectively; c_k and c_ε are determined experimentally. In the current implementation of finite volume discretization, the filter width is related to the mesh cell. Near the wall, however, and in order to capture and resolve the smallest turbulence scales, the filter width is adjusted to be min ($0.04y$, Δ) where y is the distance between the cell center and the closest wall. The dynamic Smagorinsky-Lilly model does implement a fixed value for c_s and suggests a method to derive its value dynamically from the resolved field [8].

Wind Tunnel Pressure Records. The wind tunnel data considered here were reported by [4]. The model is equipped with over 400 pressure taps, as depicted in Fig. 2, Cp time histories were sampled at 400 Hz for 60 seconds and obtained at 36 wind directions between 0^{o} and 180^{o} at 5^{o} intervals by setting up the model at the center of the circular base and incrementally rotating the base. The test section included large spires to create wind gusts at the wind tunnel entrance, as well as roughness elements as tall as the building height H upstream. A shorter $0.1H$ roughness element in the vicinity of the model was used to simulate the ABL. The roof pressures were obtained via a high speed pressure scanner connected to the tap tubing and then normalized via the dynamic pressure obtained at the same eave height H to yield Cp. The full-scale hourly wind speed was 10.15m/s and was used in the production of the wind tunnel test data. Two sets of pressure taps were located at the center and the edge of the upstream building's roof-edge, as seen in Fig .3, and their locations are listed in Table 1.

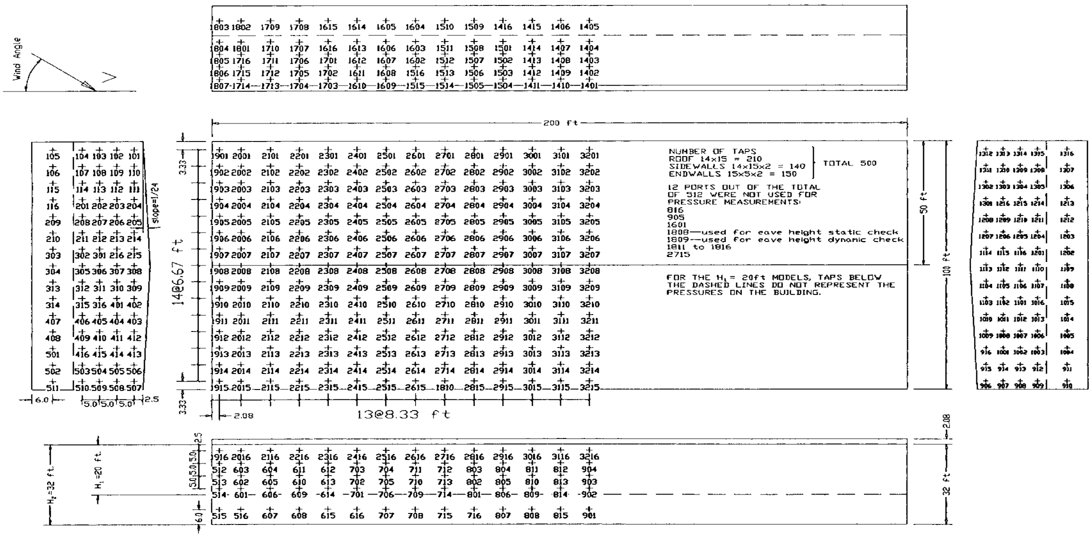

Fig. 2. Pressure taps location with respect to the building roof and along the walls.

Table 1. Location of the data points considered in the study.

Center	*x(H)*	*y(H)*	*z(H)*	**Side**	*x(H)*	*y(H)*	*z(H)*
1908	0.1040	1.0651	0.0000	**1901**	0.1040	1.0043	2.3345
2008	0.5205	1.0651	0.0000	**2001**	0.5205	1.0043	2.3345

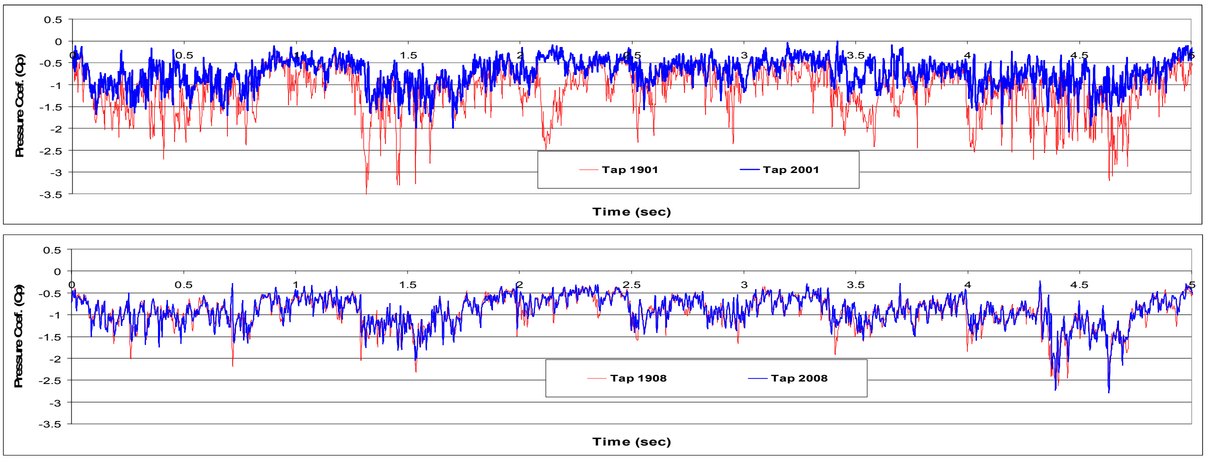

Fig. 3. Wind tunnel time Series of Cp at two sets of roof taps, side and center

These records were tested for quality [4] as numerically simulated records on the order of 60 seconds are difficult to obtain. It concluded that, within sample errors that increase with decreasing record length, a record length of a few seconds can be reasonably representative of the mean and variance of the pressure coefficients.

Numerical Analysis. Computational domain is set up to simulate the flow over a 1/200 scale model of the 10H x 5H x H low-rise building with a 1/24 roof slope. H is the full scale building's 6.1 m (20 ft) eave height. The C_p time histories of the taps presented in Table 1, as well as the upstream velocity components at the model height H are monitored and recorded. A computational domain of 130H x 105H x 13.5H was constructed around the building. It is bounded by the ground no-slip surface, the open terrain power law velocity inlet ($u = U(y/270)^{0.16}$) at a distance of 20H upstream, the outlet pressure at 100H downstream of the building's leeward face, the two side slip walls at 20H, and the upper slip wall at 40H above the building. This domain is fitted with 60 structured blocks to better control the mesh size and admit the boundary-layer fine resolution. It is comprised of 1,200,000 hexagonal finite volume cells with wall refinements of 0.0075H smoothly staggered at 1.15 to 1.2 successive length ratios away from the walls. The overall mesh count is nearly

136x170x54 subtracting the building (44x50x44). Fig. 4, depicts the computational domain fitted with the surface mesh of the building. The incoming fluctuations are modeled by using a random flow generator where the flow components are computed and synthesized with a divergence-free velocity vector comprising 100 Fourier harmonics, with an initial turbulent intensity of 0.1.

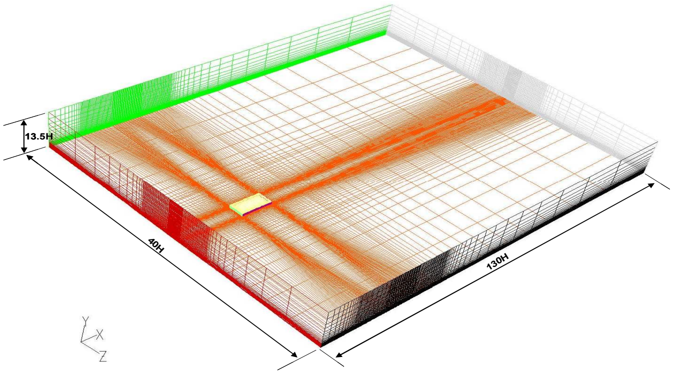

Fig. 4. Computational domain mesh dimensions in building height units.

A second-order spatial and central time scheme with a time step of $4x10^{-5}$ seconds is used. This time step is within the range of the Courant-Fredric stability requirements, particularly in the vicinity of the model $(CFL = \Delta t\, u_{local} / \min(\Delta x, \Delta y, \Delta z) < 3)$. The normalized wall distance ($y^+ = u_w y / \nu$, where $u_w = \sqrt{\tau_w / \rho}$ and τ_w is the wall shear) is iterated in several trials of mesh construction and analysis to produce $y^+ < 10$. The achieved convergence levels for the continuity and momentum residuals were targeted to reach 10^{-6} and 10^{-8}, respectively, at each time step. The velocity pressure coupling is achieved via the SIMPLE algorithm and uses on average 30 inter-iterations. The building drag and lift coefficients were also recorded and their history plots are used as an indicator of the stability of the computed data. Fig. 5, depicts the time history of those coefficients. It shows the flow needed 0.065s to become stationary. This time is equivalent to the flow "transfer time" to reach the building front (u_{avg}(H)=9.5m/s, L=0.6096 m). Contours of the magnitude of the velocity field at the end of 0.1736 seconds (4340th time step) are depicted in Fig. 6. They illustrate the formation of the upstream vortex core, roof separation and reattachments zone, building wake, as well as the free shear layer. The line plot of the main shear (u_x) at several locations illustrates this further. It shows the presence of a reverse flow upstream confined to the ground and extended nearly 2H length. Another reverse flow confined by the roof extends to 1.5H length. Behind the model, a mixing shear layer is formed at the edge of the wake far from the ground, and the wake roll up vortex region extends over 5H lengths. The computed temporal velocity record at the eave elevation H and upstream at $10H$, as well as the computed component spectra is depicted in Fig. 7. The energy-containing eddies are centered near 0.15 and extend to 0.35 normalized frequency, $f* = f.H / V_\infty$ where f is the frequency and V_∞ is the flow velocity. Axial velocity fluctuation dominates the lateral and vertical components. The input flow velocity was perturbed via a divergence-free spectrum method to simulate incoming flow turbulence. This perturbation is captured in Fig.7, upstream of the model; the computed local turbulent intensity is I=0.045 (Ix=0.05, Iy=0.06, Iz=0.038).

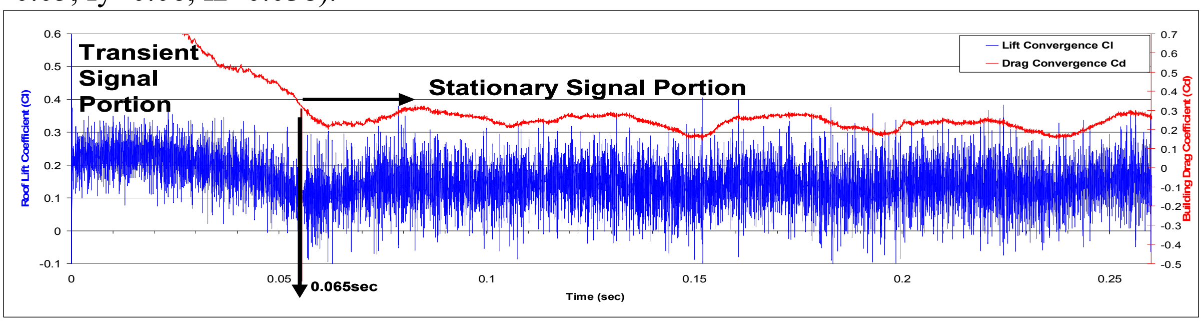

Fig. 5. Results of the Global Building Lift and Drag Coefficients.

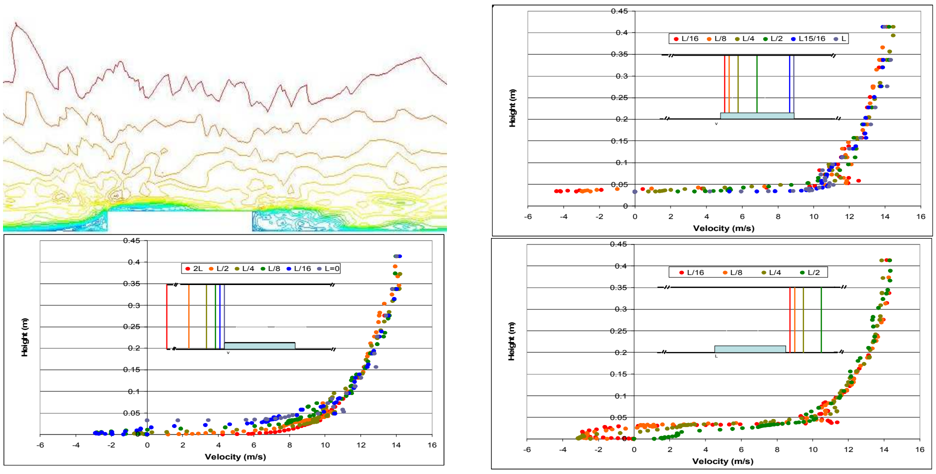

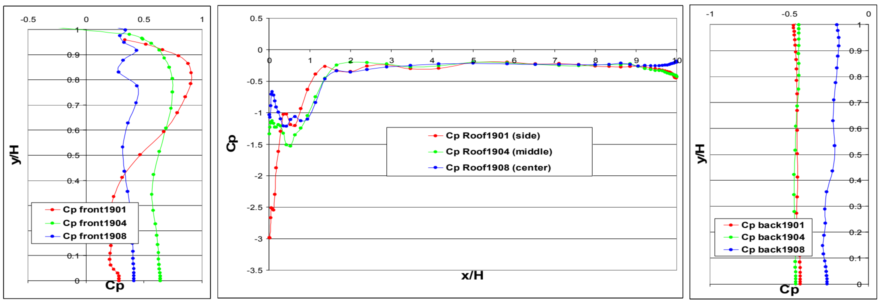

Fig.6. Cp plots at the side, quarter and center lines.

The computed Cp time histories for the two taps located at edge are depicted in Fig. 8. For a 0.5 s computed interval, minimum, mean, standard deviation, and the number of peaks for these taps compared to the 60 s time record wind tunnel data are given in Table 2, below. The data in general has similar trends as the wind tunnel data. The velocity shows, however, a tendency to drop by 0.8% due to the turbulence introduced in the model and thus it could produce lower instantaneous dynamic pressure. This may reduce the peak values down to a level closer to those obtained in the wind tunnel. The mean values are well behaved and compare reasonably well with the wind tunnel values; a longer computed record could improve the agreement. The frequency of occurrence of peaks is important; a peak is accounted for if the pressure coefficient value drops below one standard deviation. Those numbers are compared to their counterparts obtained from the wind tunnel data at different lengths. They compare favorably with records of up to 8 seconds. Fig. 9 shows the mismatch between the wind tunnel axial flow profile and the one resulting from the numerical simulation at one building length distance upstream. It also shows the large mismatch in the turbulent intensity which is almost 4 times higher in the wind tunnel. Due to the low frequency resolution in the wind tunnel, the frequency values are believed to be better in the numerical simulation. The augmentation of this intensity while achieving a tight convergence and matching the flow profile is proposed as future work.

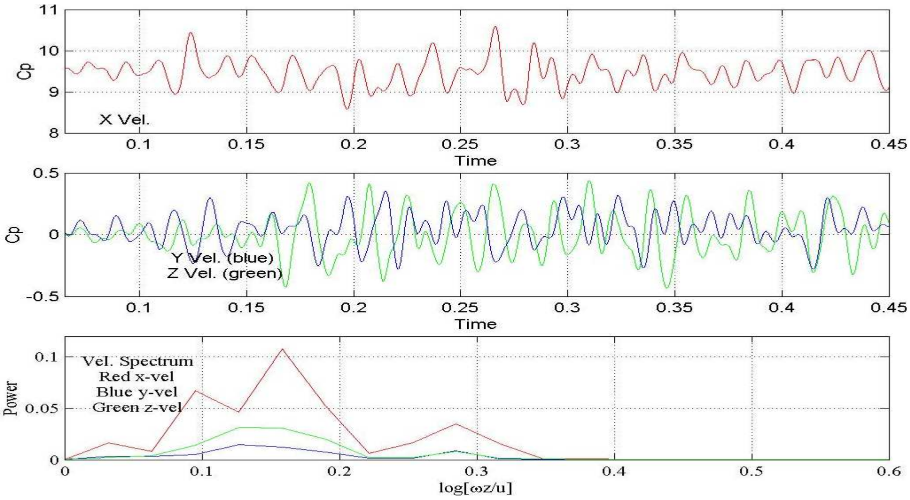

Fig. 7. Computed velocity components at L distance upstream and at H altitude, and their spectra.

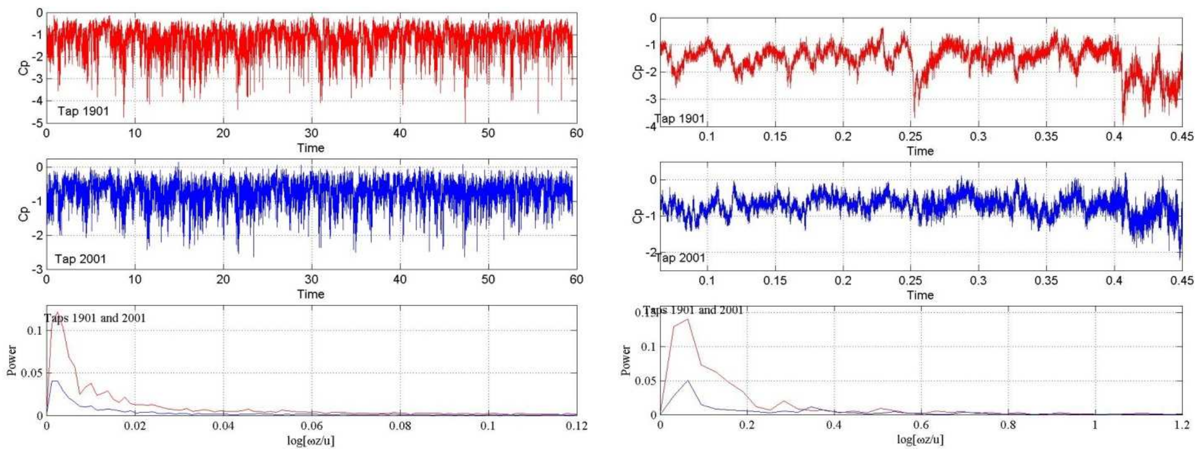

Fig. 8. Wind tunnel (left) numerical simulation (right) comparison for Cp values and its spectra

Table 2. Wind tunnel numerical simulation comparison for Cp values

Tap Number	Min 0.5sec Comp.	Min 60 sec Exp.	Mean 0.5 sec Comp.	Mean 60 sec Exp.	St. Div. 0.5sec Comp.	St. Div. 60sec Exp.	#peaks 0.5sec Comp.	#Peaks 60sec Exp.
Tap 1908	-2.0897	-3.0863	-0.9393	-0.9408	0.2733	0.3756	1270	3715
Tap 2008	-2.0433	-2.8688	-0.8308	-0.9151	0.3193	0.3639	1365	3795
Tap 1904	-2.1582	-3.1894	-1.0387	-0.9742	0.2424	0.3858	1207	3678
Tap 2004	-1.7960	-3.1722	-0.9033	-0.9345	0.2810	0.3857	1466	3672
Tap 1901	-3.6773	-5.0847	-1.4027	-1.1940	0.3880	0.5741	1242	3432
Tap 2001	-1.4221	-2.6283	-0.6779	-0.9345	0.2372	0.3418	1314	4624

Conclusion. This work suggests the potential feasibility of CFD utilizing Large Eddy Simulation to simulate pressure time histories obtained by wind tunnel measurements. Mean pressures compared reasonably well with the corresponding wind tunnel measurements, but peak values were underestimated significantly. The current computations resulted in a turbulent intensity near 0.05, less than quarter the value reported for the wind tunnel. Wind tunnel turbulence intensity is augmented by the inclusion of spires and elemental roughness. While adding spires and roughness elements in the simulation is computationally cumbersome, increasing turbulence intensities and avoid filtering it in the upstream can be achieved in the future. This work also demonstrates the tremendous length of time required to achieve a record length equivalent to that obtained in the wind tunnel.

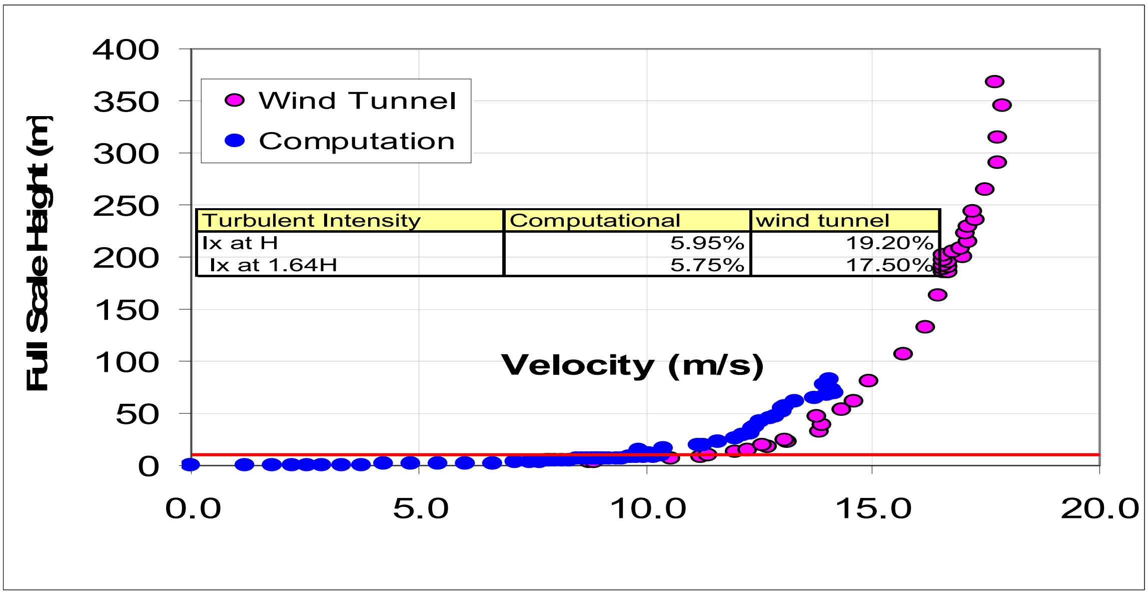

Fig. 9. Numerical-wind tunnel comparison for velocity profile and turbulence intensity.

It suggests, however, that a much shorter time record length of a few multiples of the transfer time through the domain could be computationally feasible and adequate for some purposes, although not for design, since sampling errors inherent in such a short record could be considerable. The simulation took 1.1 to 1.2 minutes of CPU time per time step on the quad dual 2.4GH processors (each time step took 25 to 30 inner-loop iterations to achieve the desired residuals of $1.0E^{-6}$ and $1.0E^{-8}$ for the continuity and velocity components respectively). At a mean flow rate of 10m/s and with a constructed domain length of 130H (H is the building height at 20ft) the total transfer time nearly 0.4 second. Thus the minimum simulation CPU time necessary is nearly 62 days for one passage and 125days for two passages utilizing 4 cores. This time could be halves by increasing the number of the processor providing low latency and higher Infiniband core and nodes communication via MPI parallel application.

Acknowledgments. This work is partially supported by NIST under grant number SB1341-05-W-1276 NIST. Masdar Institute of Science and Technology (MI) support is highly acknowledged.

References

[1] Main, J. A., and Fritz, W. P. (2006), *Database-Assisted Design for Wind: Concepts, Software, and Examples for Rigid and Flexible Buildings*, NIST, March 2006, 99 page CODEN: NBSSES.

[2] Sadek, F., Diniz, S., Kasperski, M., Gioffrè, M., , and Simiu, E., (2004), “Sampling Errors in the Estimation of Peak Wind-Induced Internal Forces in Low-Rise Structures”, *J. Engrg. Mech*. Vol. 130, pp. 235-239.

[3] Adina R & D, Inc. (2006), “Adina Theory and Modeling Guide: ARD 06-9 November 2006”, page 291.

[4] Ho, T.C.E. , Surry D., Morrish D., .Kopp, G. A. (2005) “The UWO contribution to the NIST Aerodynamic database for wind loads on low building: Part 1. Archiving format and basic aerodynamic data” *Journal of Wind Engineering and Industrial Aerodynamics* 93 1-30, 2005.

[5] Murakami, S., (1992), “Comparison of Various Turbulence Models Applied to a Bluff Body”, 1st International Symposium on CWE, Tokyo, 1992. *J. of Wind Engineering*. No.52 Aug.

[6] Lesieur, M., Metais, O., Comte, P. (2005), “Large Eddy Simulation of Turbulence”, Cambridge University Press 2005, ISBN 0-521-78124-8

[8] Holscher, N. (1996), “A non-linear approach for the aerodynamic admittance of wind pressures,” *Third International Colloquium on Bluff Body Aerodynamics & Applications*, July 28-August 1, 1996, Virginia Teach, Blacksburg, Virginia, pp. A VI 23-A VI 28.

[7] Smagorinsky, J. (1963), “General Circulation Experiments with the Primitive Equations. I. The Basic Experiment”, *Month. Wea. Rev.*, 91:99-164, 1963.

Mechanical Engineering and Materials
10.4028/www.scientific.net/AMM.152-154

Large Eddy Simulation of Wind Loads on a Low-Rise Structure and Comparison with Wind Tunnel Results
10.4028/www.scientific.net/AMM.152-154.1806